
Article:
Elsakka, M.M. orcid.org/0000-0002-4937-8843, Ingham, D., Ma, L. et al. (1 more author) (2019) CFD analysis of the angle of attack for a vertical axis wind turbine blade. Energy Conversion and Management, 182 (15 February 2019). pp. 154-165. ISSN 0196-8904

https://doi.org/10.1016/j.enconman.2018.12.054

"CFD Analysis of the Angle of Attack for a Vertical Axis Wind Turbine Blade"

Mohamed M. Elsakka[1,2], Derek B. Ingham[1], Lin Ma[1], and Mohamed Pourkashanian[1]

[1] Energy2050, Faculty of Engineering, University of Sheffield, UK

[2] Faculty of Engineering, Port Said University, Egypt

An accepted manuscript for publication in Energy Conversion and Management. The final version is available via https://doi.org/10.1016/j.enconman.2018.12.054

ABSTRACT

The Angle of Attack (AOA) of the Vertical Axis Wind Turbines (VAWTs) blades has a dominant role in the generation of the aerodynamic forces and the power generation of the turbine. However, there is a significant uncertainty in determining the blade AOAs during operation due to the very complex flow structures and this limits the turbine design optimization. The paper proposes a fast and accurate method for the calculation of the constantly changing AOA based on the velocity flow field data at two reference points upstream the turbine blades. The new method could be used to calculate and store the AOA data during the CFD simulations without the need for extensive post-processing for efficient turbine aerodynamic analysis and optimisation. Several single reference-points and pair of reference-points criteria are used to select the most appropriate locations of the two reference points to calculate the AOA and It is found that using the flow data from the two reference points at the locations 0.5 aerofoil chord length upstream and 1 chord away from each side of the aerofoil can give most accurate estimation across a range of tested AOAs. Based on the proposed AOA estimation method, the performance of a fixed pitch and the sinusoidal variable pitch VAWT configurations are analysed and compared with each other. The analysis illustrates how the sinusoidal variable pitch configuration could enhance the overall performance of the turbine by maintaining more favourable AOAs, and lift and drag distributions.

NOMENCLATURE

Symbols

C_P	Power coefficient, C_P=Power/(0.5*density*swept area*V^3)	
C_p	Pressure coefficient, C_p=pressure/(0.5*density*V^2)	
C_T	Torque coefficient, C_P=Torque/(0.5*density*swept area*V^2*turbine radius)	
$\overline{C_T}$	Single-blade cycle-averaged torque coefficient	
$\widehat{C_T}$	Peak torque coefficient	
V	Approaching wind velocity	[m/s]
V_r	Relative velocity	[m/s]
V_∞	Undisturbed flow velocity	[m/s]
y^+	Dimensionless wall distance, y^+=cell height*frictional velocity/kinematic viscosity	

Greek symbols

α	Angle of attack	[deg]
ϕ	Azimuthal angle	[deg]

Abbreviations

AOA	Angle of Attack	[deg]
BEM	Blade Element Momentum	
CFD	Computational Fluid Dynamics	
HAWT	Horizontal Axis Wind Turbine	
LES	Large Eddy Simulation	
RANS	Reynolds-Averaged Navier–Stokes	
RMSE	Root Mean Square Error	
SST	Shear Stress Transport	
TSR	Tip Speed Ratio	
UDF	User Defined Function	
VAWT	Vertical Axis Wind Turbine	
VP	Variable Pitch	
ZFP	Zero Fixed Pitch	

1 INTRODUCTION

In recent years, there has been a notable increase in the number of investigations on the Vertical Axis Wind Turbines (VAWTs) and this has given the VAWT technology a new rebirth. While the Horizontal Axis Wind Turbines (HAWTs) have acquired the major portion in the wind power market, the VAWT concept is estimated to play a dominant role in the next 2–3 decades [1]. In particular, the VAWTs feature many potential advantages, especially for operating in the urban environment and the offshore floating platforms [2]. However, in general VAWTs currently suffer from lower efficiencies in comparison with the HAWTs [3]. Therefore, an intensive research on improving the aerodynamics of the VAWTs have been observed in recent years.

The VAWTs can be classified as two types of configurations, i.e. the Savonius and Darrieus designs [4], [5]. The Darrieus designs rely on the lift generated from the aerofoil-profiled blades while the Savonius designs are driven by the drag from bucket shaped vanes [6]. Generally, Savonius turbines have lower efficiencies although they have better startup characteristics than the Darrieus turbines [4]. However, the Darrieus type VAWTs offer significant advantages over Savonius turbines, and have a much higher power coefficient and suitable for large scale operations [4]. Since the driving elements of Darrieus type VAWTs are the aerofoils-profiled blades, the turbine performance is strongly dependent on the incident angle of the flow relative to the blade chord, also is referred to as the baled Angle of Attack (AOA). Therefore, an accurate estimation of the incident flow direction and the AOA during turbine operation is critical for turbine design optimisation [7].

There is intensive research interest on improving the straight bladed VAWT efficiency through controlling the blade AOA during its rotation around the vertical axis, especially for high efficient operations at low Tip Speed Ratios (TSRs) which rely on the appropriate design of the turbine blade pitching angle [8] or applying the variable pitch to the blade control [9]. For example, the variable pitch based on the cycloidal kinematics has been widely investigated [10]–[12]; Erickson et al. [13]

obtained 35 % enhancement in the turbine efficiency using a first-order sinusoidal pitch; Liu et al. [14] achieved a some improvement in the turbine performance using sinusoidal pitch with low amplitude; and Paraschivoiu et al. [15] found that the turbine annual energy production could be increased by about 30% using an optimized variable pitch based on a suggested polynomial of sinusoidal functions.

The interactions between the wind and the VAWT rotations lead to very complex time-variant aerodynamic phenomena around the spinning blades. The use of the overall turbine power as a function of turbine TSR is the most common method for the analysis of the aerodynamic performance of VAWTs, and it can illustrate the variation of the power coefficient at different TSRs. Although several studies have analysed the instantaneous power and/or torque coefficient over one cycle [16]–[22], a more detailed analysis is required to understand the reasons for the differences in the power generation efficiency between different turbine designs, in order to gain a better understanding of the complex aerodynamic characteristics of the VAWTs.

The interactions between the wind and the VAWT rotations lead to very complex time-variant aerodynamic phenomena around the spinning blades. Although several studies have analysed the instantaneous power and/or torque generation over one rotating cycle [16]–[22], a more detailed aerodynamics analysis and in particular the effects of instantaneous AOA are required in order to obtain an in-depth understanding of the aerodynamic reasons for the differences in the power generation efficiency between different turbine designs of the VAWTs. A range of different-fidelity analyses has been used to investigate both fixed and variable pitch VAWTs and the estimations of the AOAs. These include the streamtube based models [23]–[25], the vortex method [26], [27], the Computational Fluid Dynamics (CFD) analysis [17], [20], [21], [28]–[31], and the high-computational cost Large Eddy Simulation (LES) [22], [32]. However, the 2D CFD analysis, based on the Reynolds-averaged Navier–Stokes (RANS), is widely used because of its reasonable accuracy and moderate

computational cost [28]. In the blade aerodynamics analysis, the AOA could be simply estimated assuming that the approaching wind velocity to the blade is constant and parallel to the undisturbed wind flow velocity. This simple calculation ignores the effects of the rotor on the flow and in particular the blade-wake interactions existing in the VAWT operation, which can lead to a significant error in the prediction of the performance of the turbine blades. While this simplified calculation of the AOA is widely used [18]–[20], [33]–[37], a more realistic estimation of the AOA is needed that takes into account the variation of the magnitude and direction of the approaching wind velocity vector to the blade at different azimuthal positions. Kozak [38] calculated the AOA based on the CFD data using two different methods and these are based on the calculated lift coefficient or the pressure ratio between the suction and pressure sides of the blades. However, his validation of these methods was limited to the study of a pitching motion with a geometric AOA between 0° and 8°. Bianchini et al. [39] used the CFD data for the estimation of the AOA based on the location of the pressure peak by comparing it to the location of the pressure coefficient peak obtained by the panel method. In order to account for the virtual camber effect, the original aerofoil coordinates are transformed to a virtual aerofoil and then the panel method is used for the pressure coefficient calculations [39]. Although this method has a good agreement with the Blade Element Momentum (BEM) results, it involves many intermediate tasks. Edwards et al. [7] presented an estimation method of the corrected AOA based on the cycle-averaged CFD velocity flow-field. This method involves discarding the distorted velocity near the blade trajectory then interpolating the flow-field. While this method provides a good estimation of the AOA, it ignores the instantaneous variation of the velocity flow field and involves many intermediate tasks. Gosselin et al. [17] claimed a good estimation of the AOA using CFD data based on the averaged velocity vector at a single point located on the tangential trajectory at a distance of two-chord lengths in front of the blade.

However, a distance of two-chord lengths appears to be large, especially for high solidity turbines where the chord to radius ratio is quite high.

It is noted that most of the estimation methods of the AOA that are available in the literature have two common drawbacks, namely (i) the lack of a reference for comparison and validation of the methods and thus can lead to relatively large errors, and (ii) the need for extensive post-processing. This paper presents a new method for the estimation of the AOA which uses the CFD simulated flow field data at two well-selected reference points around the blade. The new method has a minimal error and more accurate estimation of the AOA compared to all the existing method tested. In addition, the new method could be integrated into the CFD solver to provide a computational inexpensive calculation in order to extract the instantaneous AOA variations along the blade flying path for efficient blade aerodynamic analyses and optimization. Finally, the new method has been applied successfully to the evaluation of the lift and drag coefficients for a fixed and a variable pitch two-bladed VAWT configurations in order to analyse the differences in the performance between the two configurations.

2 PROPOSED METHODOLOGY FOR AOA ESTIMATION

In this paper a new method of estimating the AOA for VAWTs based on the flow field at two reference-points upstream the turbine blade is proposed. Since the relative approaching flow velocity and direction to the blade are very complex and constantly changes, it is critical to select correct reference points where a representative incident flow direction can be obtained for the correct estimation of the blade AOA. In order to find these reference points around the blade that can result in an accurate and easy calculation of the AOA for VAWTs, the fluid flow around a static aerofoil with a range of set AOAs has been used as a test and validation case. CFD simulations have been performed to obtain the flow field data around the aerofoil at several selected reference-points, and these data are used to calculate the AOAs around this static aerofoil and compared with

the set AOAs. The normalized Root Mean Square Error (RMSE), based on the differences between the calculated and the prescribed AOAs, is calculated and used to select the most suitable reference-point locations with a minimal error, as will be discussed in Sections 2.3. It is found that using the flow data from the two reference points at the locations 0.5 aerofoil chord length upstream and 1 chord away from each side of the aerofoil can give most accurate estimation across a range of tested AOAs. Then, these selected reference-point locations are used to estimate the angle of attack around a VAWT blade which have successfully predicted the AOAs with good accuracy, as discussed in Section 3.2. This proposed method for the estimation of the AOA is illustrated in Figure 1.

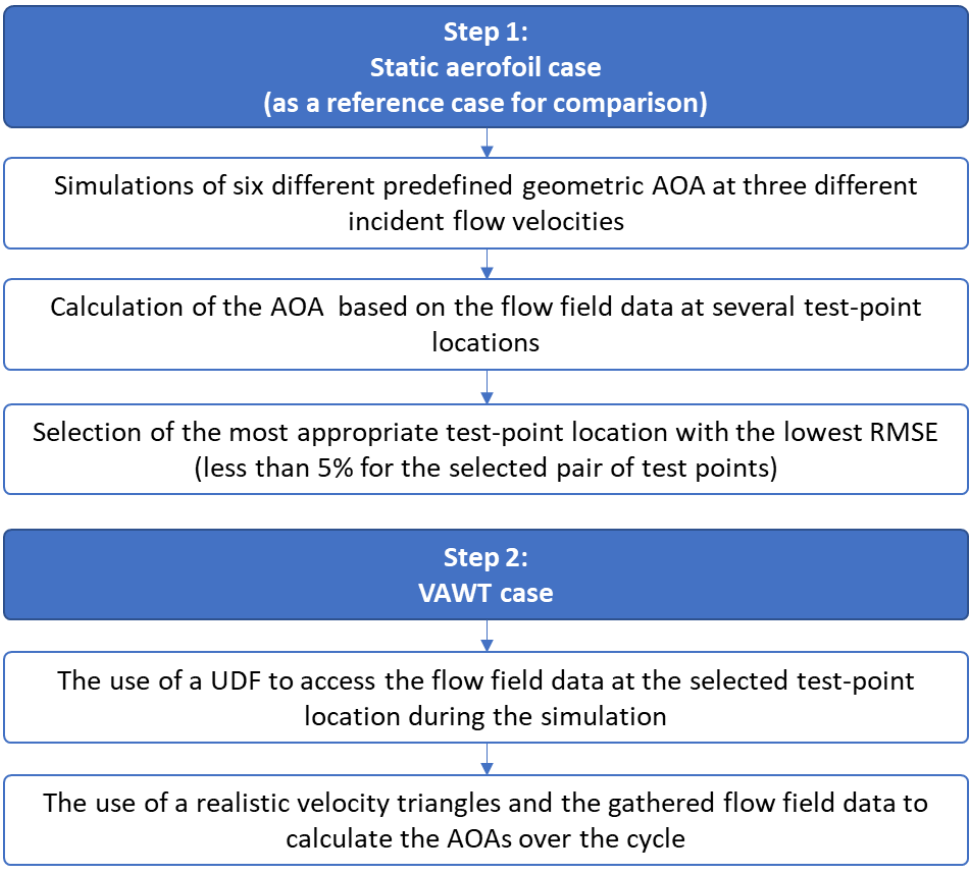

Figure 1 A flow diagram for the proposed method for the estimation of AOA.

2.1 Estimation of the AOA for a static aerofoil

The flow around a static aerofoil is considered with a range of prescribed geometric AOAs as shown in Figure 2 (a) where the NACA0015 aerofoil with a chord length of 0.225 m is used. This range of AOAs includes the angles between 0° to 25° with 5° increment. The flow conditions and aerofoil geometry are chosen according to the reference VAWT case that is discussed in Section 3.1.1. The static aerofoil simulations are performed at different incident flow velocities of 7, 14, and 21 [m/s] and these correspond to the average relative velocities around a VAWT blade that operates at TSRs of 1, 2, and 3, respectively, when rotating across a mainstream flow with a velocity of 7 m/s. This range of TSRs is chosen to cover the optimum operation range of moderate solidity VAWTs. Due to the lack of experimental data at the chosen flow conditions, the data from the widely validated XFOIL software [40] is used to validate the CFD model. XFOIL has been developed for the prediction of the aerofoil characteristics at low Reynolds numbers. This is established by incorporating both the integral boundary layer and transition equations along with the potential flow panel method. Morgado et al. [41] compared the XFOIL predictions to both of the experimental and CFD data for the aerofoil characteristics at low Reynolds number and they reported that XFOIL is an excellent analysis tool for aerofoils. The accurate predictions on using XFOIL makes it reasonable to be used for the verification of other numerical methods, including CFD, especially when there is a lack of experimental data for the desired flow conditions.

A commercial CFD solver, namely ANSYS FLUENT, has been used with double precision in the steady mode in order to model the flow around the aerofoil. The pressure based coupled algorithm is used to solve the momentum and continuity equations while the SST k-ω turbulence model is used to account for the turbulence effects. The second-order upwind interpolation scheme is employed for the discretization of the momentum and turbulence equations. The solution is iterated upon until the normalized residuals of the flow variables reduce by five orders of magnitude.

In order to impose the prescribed AOA, the whole computational domain is inclined with the prescribed AOA as shown in Figure 2 (b). The computational domain is extended to 40 chord length in the downstream direction and 20 chord lengths elsewhere in order to eliminate any effects of the domain boundaries on the flow around the aerofoil. The computational domain is divided into a circular subdomain around the aerofoil and a rectangular extended domain and a circular non-conformal interface is used to connect these subdomains. This two subdomain configuration assists in maintaining the same mesh structure and quality regardless of the changes in the imposed AOA. A full structured mesh is constructed across the domain as shown in Figure 3 (a). Figure 3 (b) shows the mesh in the vicinity of the leading edge of the aerofoil where a fine resolution is maintained around the aerofoil using an inflation zone with 110 layers, a maximum dimensionless wall distance, $y^+ <1$ and a growth rate of 1.05. y+ represents the normalized distance perpendicular to the wall and has very important role in describing the near wall flow. By maintaining y+<1, the viscosity dominated region, including the viscus sublayer, is resolved and hence a better estimation of the aerodynamic forces could be achieved.

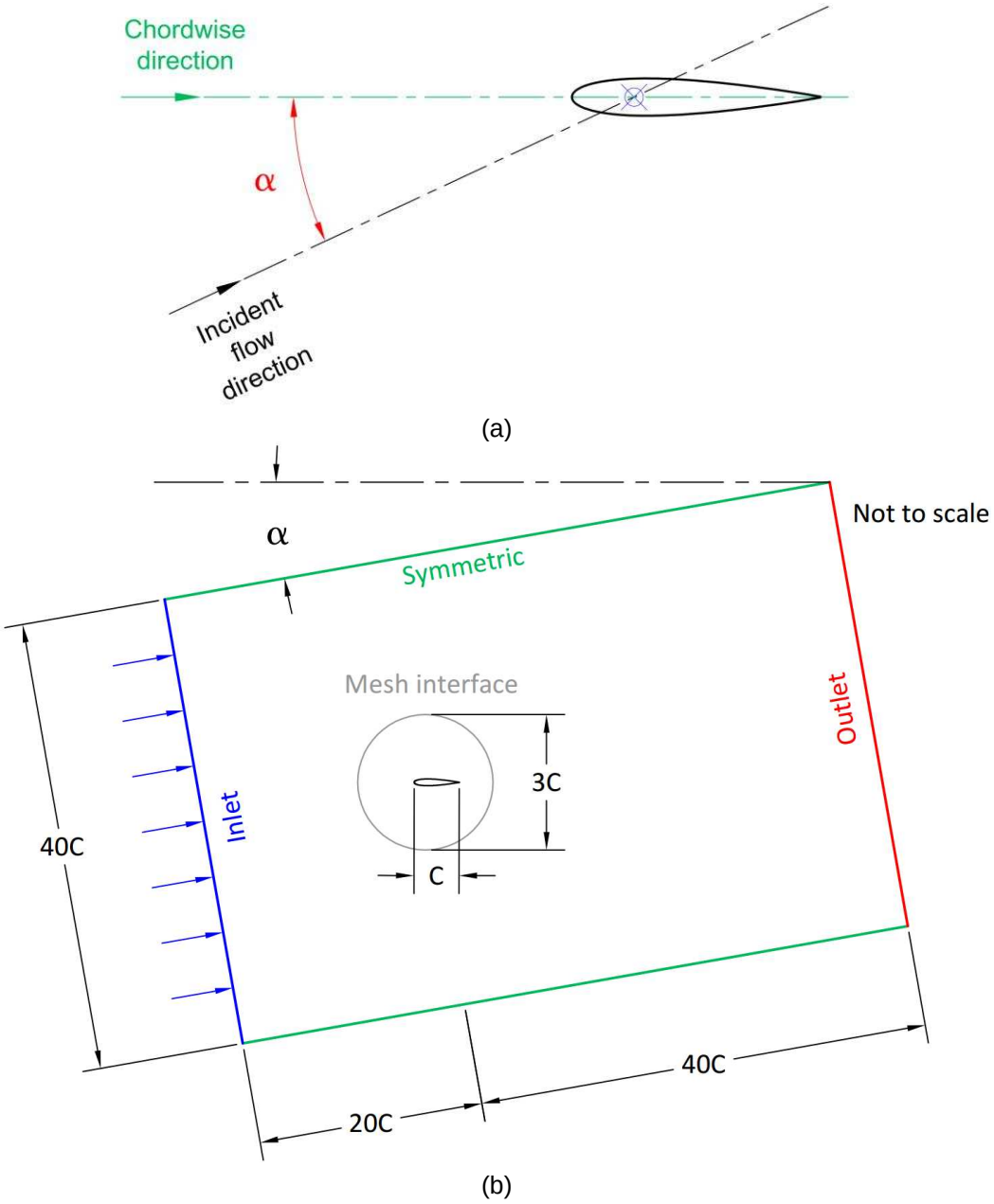

Figure 2 Schematics of (a) the incident flow around a static aerofoil and (b) the computational domain for the static aerofoil case (not to scale).

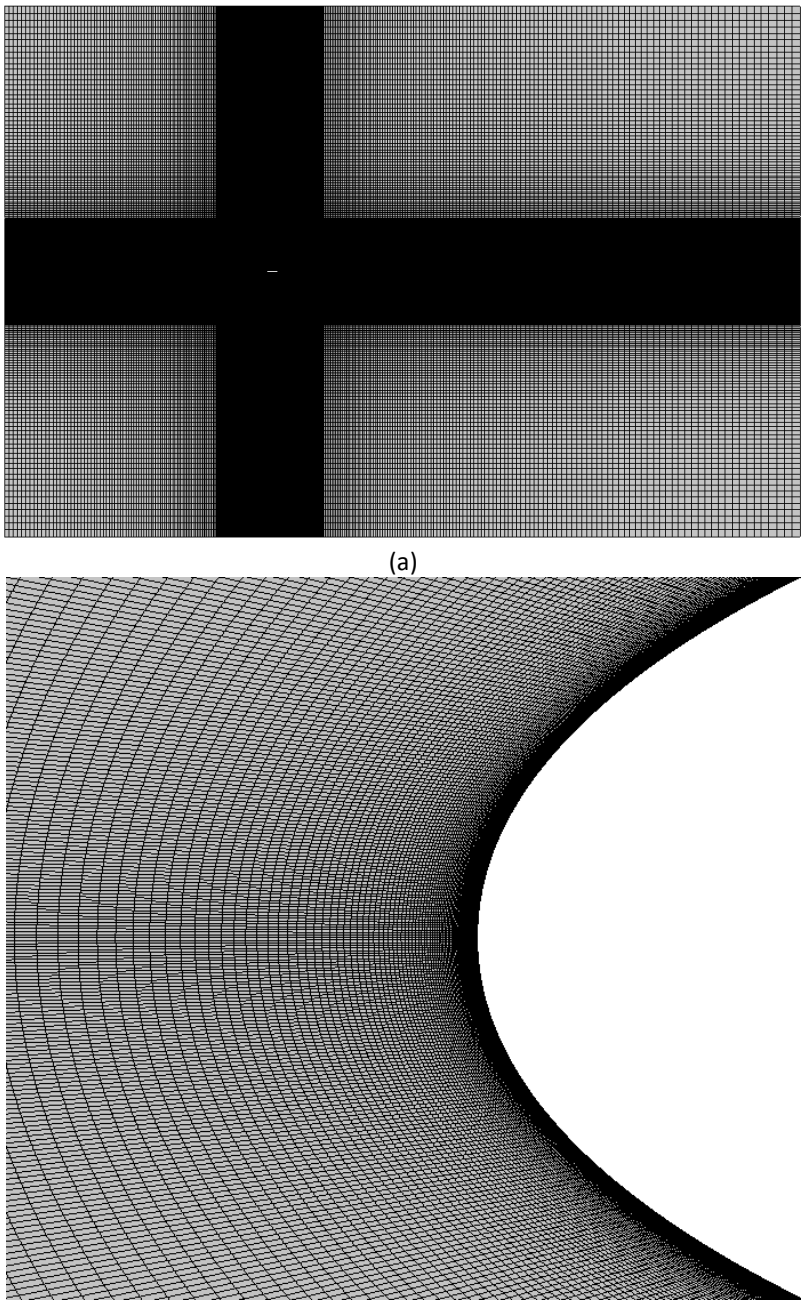

(a)

(b)

Figure 3 (a) The structured mesh across the domain and (b) Mesh clustering around the leading edge of the aerofoil.

In order to test the solution sensitivity to the generated mesh, three levels of mesh refinement are constructed with a refinement factor of 2. These meshes include the coarse mesh, baseline mesh, and fine mesh with a total number of elements 116400, 354600, and 1198400, respectively. Figure 4 shows the distribution of the pressure coefficient around the aerofoil at AOA=10° for the largest flow velocity of 21 [m/s] for the three meshes and it is found that there is no significant difference

observed in the results obtained. The reason why there are no obvious differences between different grids is that the dimensionless wall distance y+, first layer thickness has been kept less than 1, and the mesh growth rate perpendicular to the aerofoil profile is kept small in all the cases. The CFD predictions of the pressure distribution around the aerofoil depends mainly on the near wall treatment and y+. Therefore, when the computational mesh is reasonably fine, the mesh refinements in the spanwise direction or outside the inflation layer do not have a significant effect on the computational results. The baseline mesh with 354600 elements is considered for this static aerofoil study in order to reduce the computational cost while maintaining a fine mesh distribution and a reasonable accuracy, in spite of the fact that the coarser mesh could be used with adequate accuracy. However, optimizing the computational cost was not prioritized in this study. Figure 5 shows the comparisons between the CFD and XFOIL predictions of the pressure coefficient around the aerofoil for flow velocities of 7, 14, and 21 [m/s] at AOA=10°. It is observed that the differences between the CFD and XFOIL data are associated with the prediction of the laminar separation bubbles. The reason is that the SST k-ω model in the CFD simulation imposes a fully turbulent flow while the viscous boundary layer module in XFOIL accounts for the laminar to turbulent transition. However, these small separation bubbles have a negligible effect on the velocity field around the aerofoil and hence do not affect the calculation of the AOA.

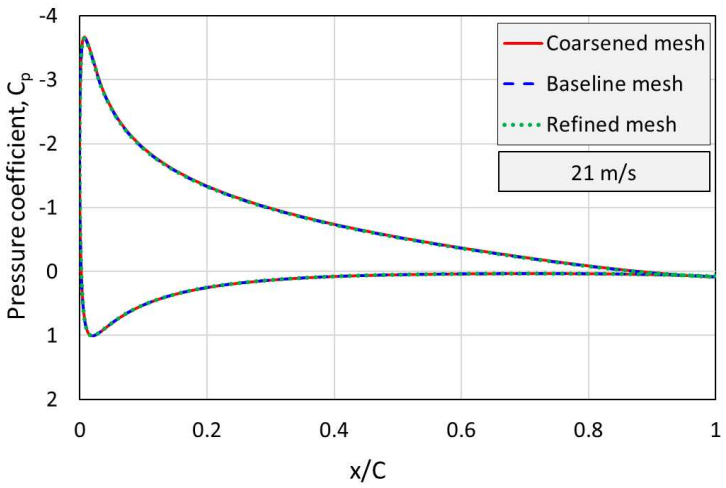

Figure 4 The effect of the mesh refinement on the pressure coefficient around the aerofoil at a flow velocity of 21 [m/s] and AOA=10°.

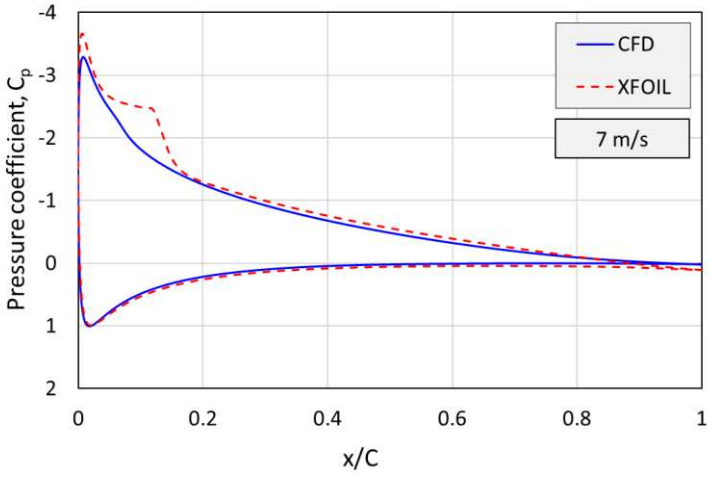

(a)

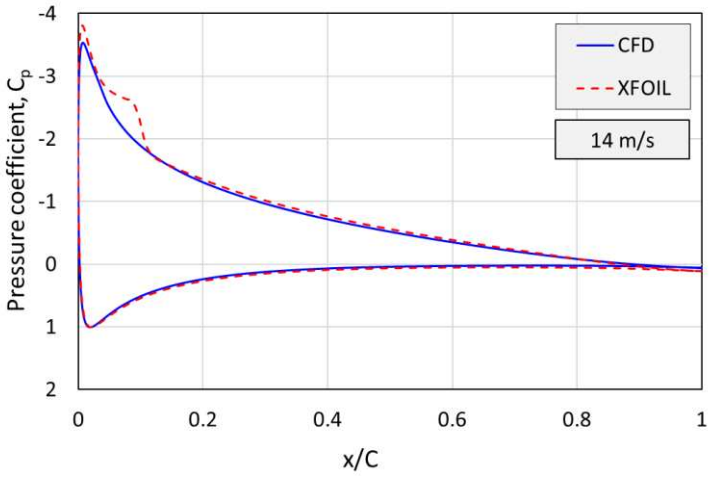

(b)

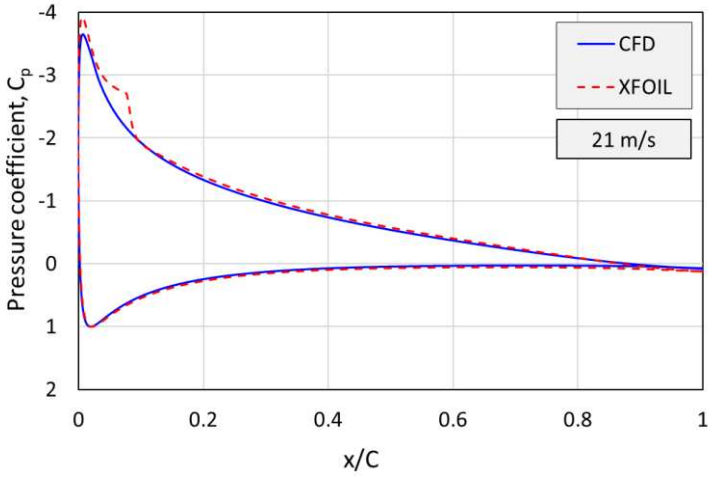

(c)

Figure 5 A comparisons between the CFD and XFOIL predictions of the pressure coefficient around the aerofoil at AOA=10°for flow velocities of 7, 14, and 21 [m/s].

2.2 Selection of the Reference-points

The proposed estimation of the AOA using CFD is based on the calculation of the inclination of the absolute velocity vector in one or multiple reference-points while the most appropriate selection of the reference-points is essential for the accuracy of the estimated AOA. The inclined flow around a static NACA0015 aerofoil is considered with six geometric AOAs, namely 0°, 5°, 10°, 15°, 20°, and 25°. In addition, three different incident flow velocities are considered, namely 7, 14, and 21 [m/s]. Both the single reference-point and pair of reference-points criteria are considered, while two groups of reference-points are selected. The first group is distributed around the chordwise direction, regardless of the incident flow direction, as shown in Figure 6 (a)**,** and in the second group, the points are distributed around the incident flow direction as shown in Figure 6 (b). Figure 7 shows the typical streamlines released from the first group of reference-points that are clustered around the aerofoil chordwise direction at AOA=10° and these streamlines show how the flow around the aerofoil is distorted, especially in the vicinity of the leading edge. The degree of distortion depends on the location of the chosen test point and hence the appropriate selection of the test point locations is essential for the accurate estimation of AOA. Several aspects are considered in the selection of the locations of the reference-points. The points should not be located in the wake of the aerofoil and the distance between each point and the aerofoil profile should not be too small to be affected by the flow distortion around the leading edge of the blade. In addition, this distance should not be too large to miss-represent the incident velocity vector.

2.3 Validation of the proposed method

In order to examine the accuracy of the AOA estimation using the flow field data at specific test point locations, the normalized RMSE is calculated based on the differences between the calculated values from the flow field data and the exact values of the six prescribed geometric AOAs. The test point locations are considered appropriate with acceptable accuracy if the corresponding

normalized RMSE is less than 5%. Figure 8 shows a comparison of the RMSE of the estimated value based on the single reference-points in addition to the normalized RMSE of the pairs of reference-points at the three selected incident flow velocities. It is clear that the pairs (i_1&j_1) and (i_2&j_2) have the lowest normalized RMSE, being less than about 5.0% and this illustrates how the pair of reference-points criterion could achieve a better estimation in contrast with the single point criterion. From a practical perspective, the pair (i_1&j_1) is considered to be more suitable than the pair (i_2&j_2) for the VAWT case due to the simpler extraction of the data around the predefined chordwise direction. One of the most accurate method of estimating AOA in the literature is from Gosselin et al. [17] using the flow field data at 2-chord lengths from the aerofoil mount point and this corresponds to employing a single reference-point (a_1) in the current study, see Figure 6 (a). In comparison, the proposed method, based on the selected pair of reference-points (i_1&j_1) as shown in Figure 6 (a), reduces the RMSE from 6.7% down to 4.4% for the incident flow velocities of 21 [m/s] and this represents a reduction of 34% in the RMSE at 21 [m/s] and an average reduction of 33.8% for the three tested flow velocities in contrast with the method employed by Gosselin et al. [17]. Furthermore, most of the other AOA estimation methods [7], [38], [39] in the literature require many intermediate and time-consuming steps which make them very difficult to be applied to the current test case under the current operating conditions for the purpose of comparisons. Therefore the location of the pair (i_1&j_1), as shown in Figure 9, is selected for the estimation of the AOA based on the velocity field around the VAWT blade as discussed in Section 3.2.

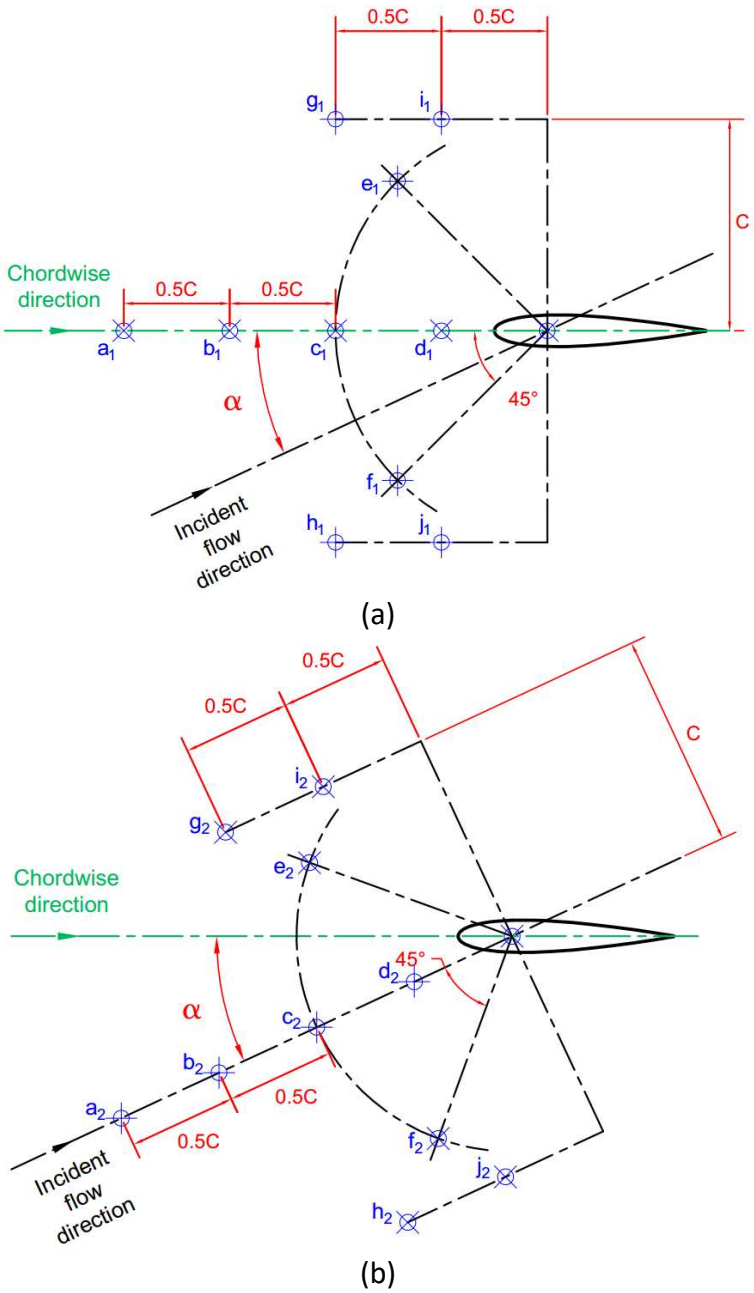

Figure 6 Locations of the reference-points.

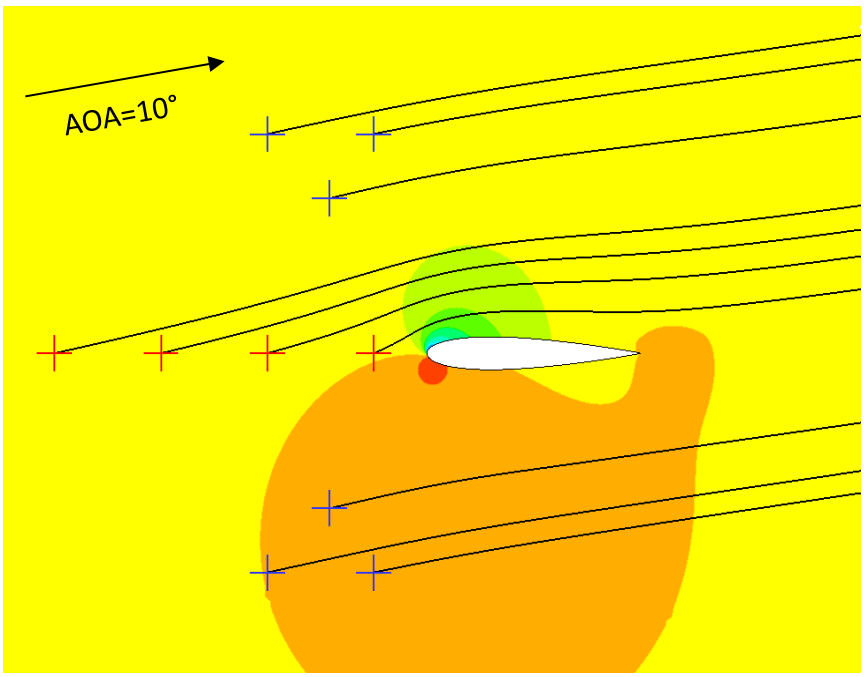

Figure 7 Streamlines released from the reference-points overlaid on the pressure contours around the aerofoil at AOA=10°.

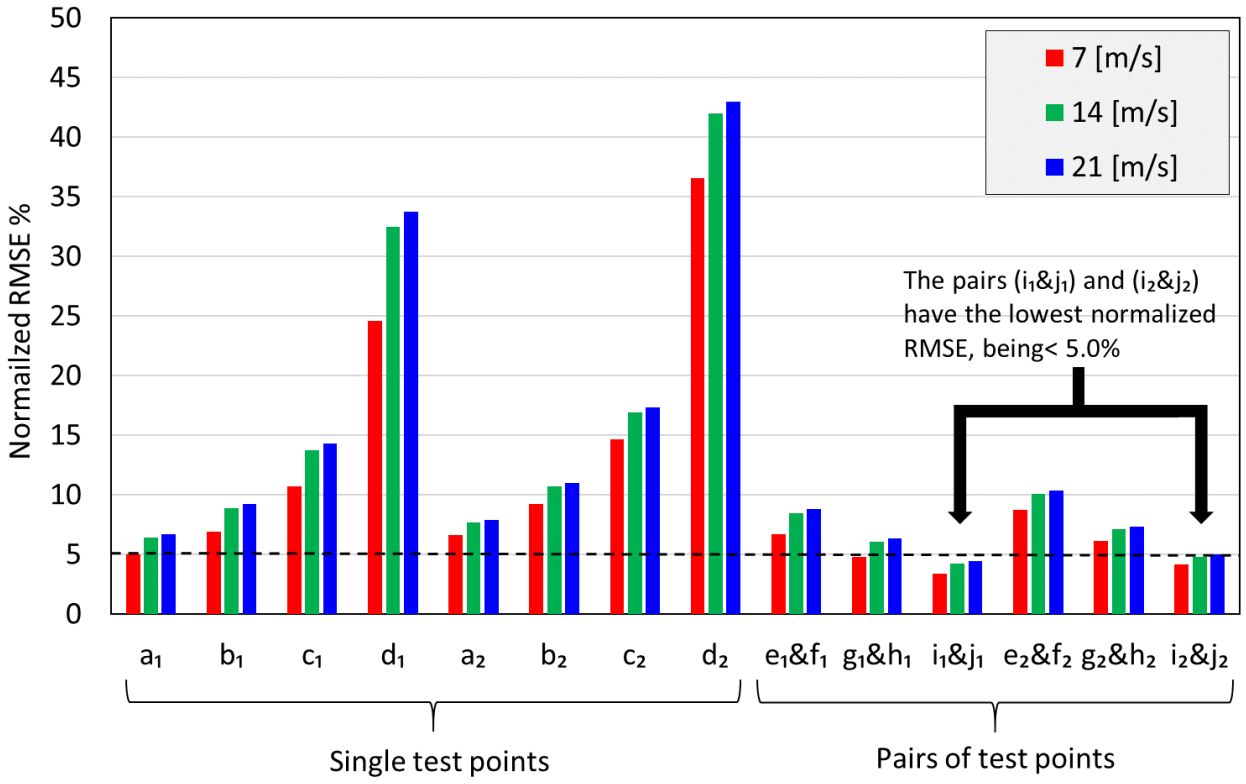

Figure 8 The normalized RMSE for the selected reference-points and pairs of reference-points against the permissible limit of 5%.

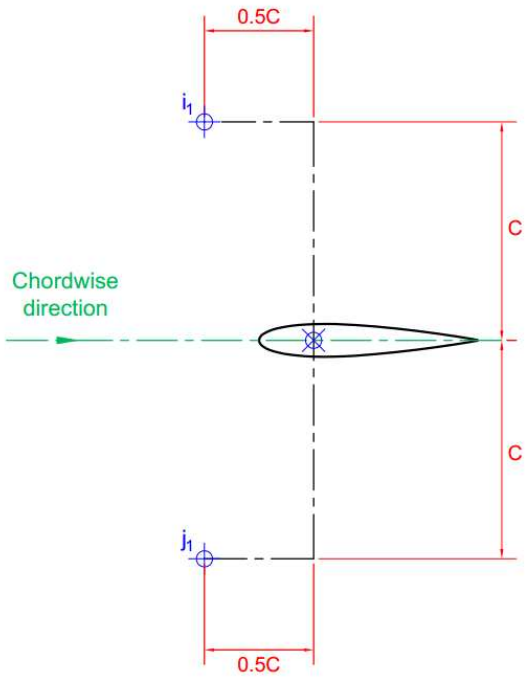

Figure 9 Locations of the selected pair of reference-points (i_1&j_1).

3 ESTIMATION OF AOA FOR VAWT

3.1 Modelling of VAWT

3.1.1 Model description

The wind tunnel experiments, carried out by Li et al. [42], are selected to validate the current CFD model. Their experimental data offers a good opportunity for the validation of 2D CFD simulations due to the inclusion of the torque contribution at the mid-span section of the blade, based on the integration of the instantaneous pressure data from a high-frequency multiport pressure scanner. In addition, their data includes the pressure distribution around the wind turbine blade at different azimuthal locations. The experimental test under consideration was based on a two-bladed VAWT model with a diameter of 1.7 m. The blade is profiled with a NACA0015 aerofoil with a chord length 0.225 m, a span 1.02 m and an aspect ratio 4.5 and each blade has an outward fixed pitch angle of 6°. A closed-circuit wind tunnel with a 3.6 m diameter open test section was used in their tests. The measurements in a wind tunnel with an open test section, i.e. without walls around the test section,

is found to minimize the blockage effects [43]. The turbulence intensity in the test section was as low as 0.5 %. More details about the wind tunnel are available in [44]. In the selected test case, the velocity in the wind tunnel test section was 7 m/s while the turbine rotated at 180 rpm and this equates to a TSR 2.29.

The flow across the mid-span plane the turbine is modelled using 2D CFD simulations, based on the RANS equations, and the SST k-ω turbulence model is utilized for the turbulence modelling as recommended in the literature [45], [46]. The use of CFD enables a deep insight into the flow characteristics in the vicinity of the blades as well as on the far-field wake and these simulations are designed to be validated against the experimental data obtained by Li et al. [42]. Their results include the single-blade contribution of the torque coefficient at the mid-span plane on the turbine, based on the integral data of the multiport pressure measurement around the blade. Despite the fact that the flow around VAWTs being three-dimensional, the 2D simulations are adequate for the prediction of the flow characteristics at the blade mid-span plane, where the flow is considered to be two-dimensional.

ANSYS FLUENT has been used and the 2D double precision version of the solver is used in the transient mode. The pressure-based coupled algorithm is considered for pressure-velocity coupling. In contrast with the segregated algorithm, the coupled algorithm features a significant reduction in the computational cost by maintaining a stable solution at high Courant numbers [47]. This means, for a given mesh, a relatively larger time step size may be used and hence the computational cost could be reduced. The second-order implicit unsteady formulation is enabled for the temporal discretization due to its improved accuracy [47]. The second-order upwind scheme is implemented for the spatial discretization of the momentum and the turbulence model equations. The sliding mesh method is used to model both of the turbine rotation and blade pitch motion, when required.

The angular velocity of both the pitch motion and turbine rotation is imposed to the corresponding subdomain using an interpreted User Defined Function (UDF) that is integrated into the solver.

The solver is allowed to perform 30 iterations per each time step and this has been found to be sufficient for reducing all the normalized residuals to, at least, five orders of magnitudes, except the turbulence kinetic energy residuals that usually reduce by, at least, four orders of magnitude. Each simulation includes five complete revolutions, while the data is recorded for post-processing at the fifth cycle to eliminate any effect of the starting unsteadiness and to ensure that a time-periodic solution is obtained. This has been found to be sufficient, under the current setup, to reduce the differences in the cycle-averaged torque coefficient between the successive cycles to less than 1.0%.

3.1.2 Computational domain and meshing topology

The flow around the two-bladed VAWT mid-span plane is modelled by a C-shaped computational domain. Figure 10 illustrates the shape of the domain, its subdomains, and the different boundary conditions. The domain extends to 8-diameters downstream of the rotation axis and 5-diameters otherwise and the selected domain size is in good agreement with those selected in several recent studies [31], [45], [48]. The domain size is selected to be large enough to eliminate the effects of the side and downstream boundaries. ANSYS DesignModeler is used for the domain assembly. The trailing edge of the aerofoil has a radius to chord of 0.19% and this has been found to have a negligible effect on the aerofoil performance. However, the use of a rounded trailing edge assists in avoiding the overprediction of the flow acceleration over the sharp corners that exist around the blunt trailing edge. In order to implement the sliding mesh method, the computational domain is constructed from several subdomains. A circular rotating subdomain is associated with the region around the turbine with a diameter of 1.5 turbine-diameters, while two small circular subdomains are constructed around the blades with a diameter of 2 chord-lengths to apply the blade pitch. In addition, a large stationary subdomain represents the region far from the turbine and the fluxes

between these subdomains are passed by means of circular non-conformal mesh interfaces as shown in Figure 10. A structured-shaped computational mesh is generated using the ANSYS Meshing software and this mesh consists of combinations of O/C/H mesh topologies. Figures 11 (a) show the meshing of the stationary subdomain. The mesh around each blade is generated with O-type mesh topology. Figures 11 (b) shows the structured mesh around the turbine blade. Further details about the baseline mesh used in this investigation are provided in Section 3.1.3.

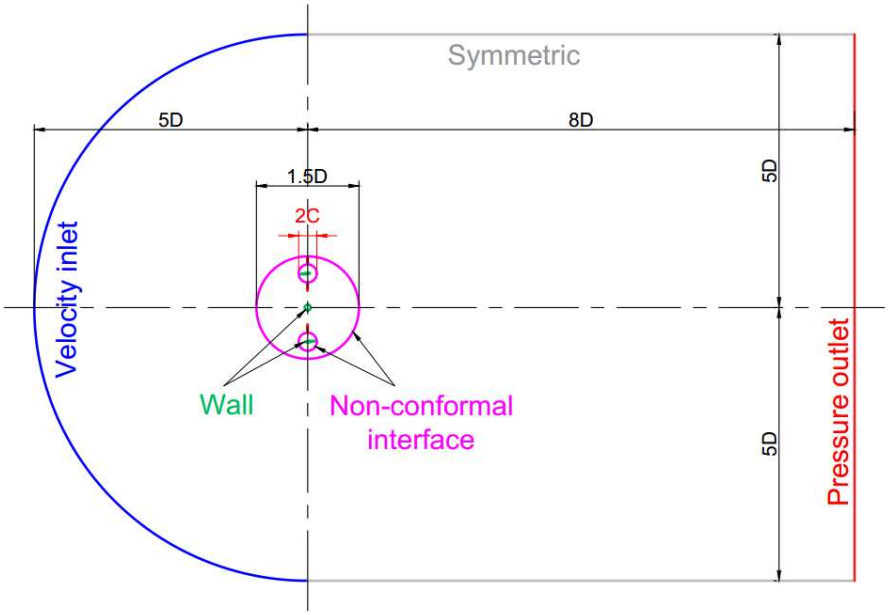

Figure 10 A schematic diagram of the computational domain, showing the boundary conditions. The distances are measured as a function of the rotor diameter, D, and the blade chord, C.

A velocity inlet boundary condition is applied to the upstream edge with a 7 m/s streamwise component and 0.5 % turbulence intensity and these values are selected to match the conditions of the experiments performed by Li et al. [42]. A zero gauge pressure outlet boundary condition is imposed to the downstream boundary of the domain and symmetric boundary conditions are applied to the lateral sides of the domain that imposes zero gradients for all fluxes across the normal direction of these boundaries. The turbine shaft and blade profiles are modelled as walls that move with the adjacent cell zones.

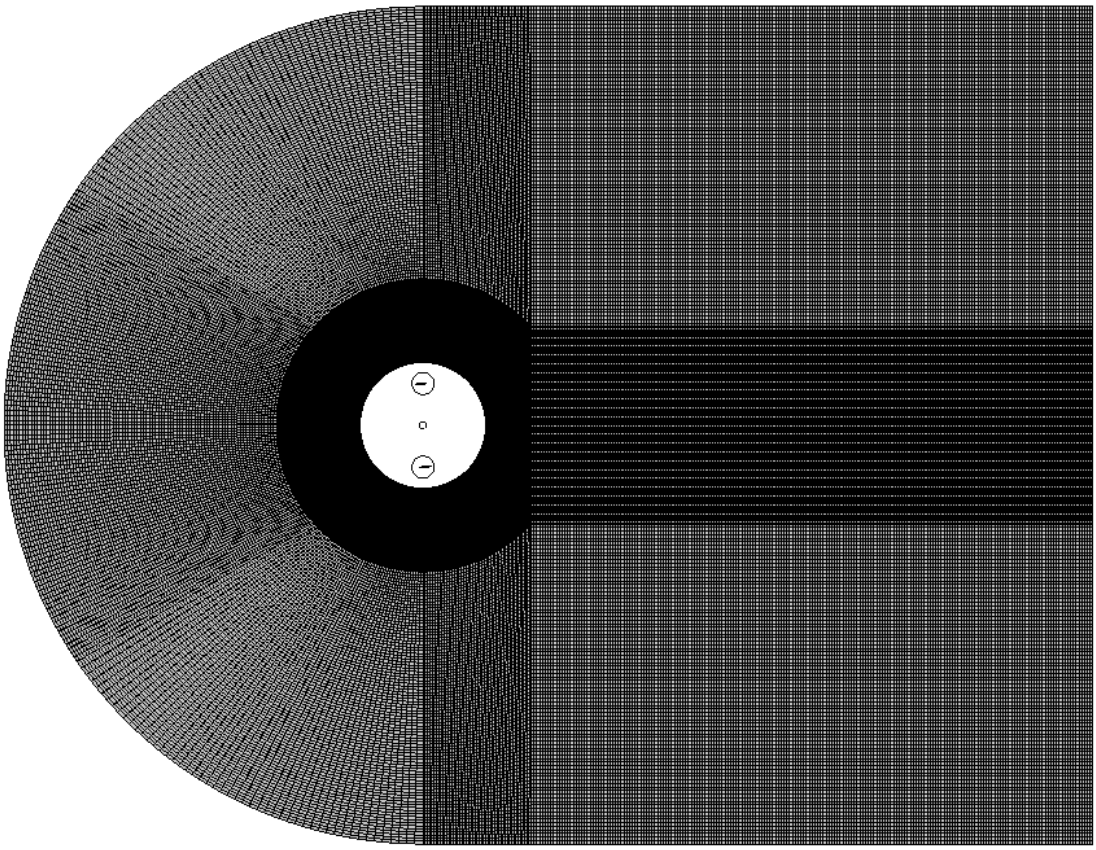

(a)

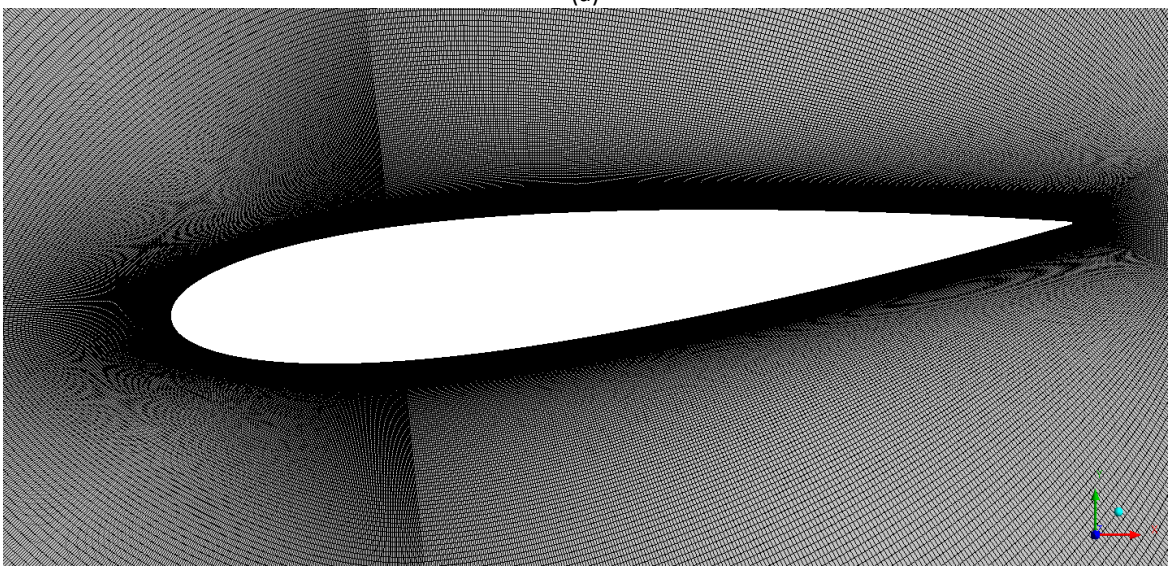

(b)

Figure 11 The mesh topology of (a) the stationary subdomain and (b) region around the blade.

3.1.3 Mesh and time step size sensitivity study

The proper selection of the temporal and spatial resolution is paramount for the modelling of the unsteady flow around VAWTs. Using the baseline mesh with a total of 701600 elements and 1260 nodes around each blade, three temporal resolutions are investigated namely, 360, 540, and 1080 time steps per cycle that correspond to resolving each degree of the azimuthal angle by 1, 1.5, and 2-time steps, respectively. Table 1 shows the effects of the different temporal resolutions in both of the single-blade cycle-averaged $\overline{C_T}$ and the peak torque coefficient $\widehat{C_T}$ over the fifth cycle. The differences in the torque coefficient are considered to be fairly insignificant as shown in Table 1 and a temporal resolution of 540 time steps per cycle is selected. In addition, two meshing attributes are considered to examine the effect of the spatial resolution. The first is the number of elements around the turbine blade where 630 and 2520 nodes per blade profile are examined along with the baseline mesh with 1260 nodes per blade profile. The second meshing attribute is the mesh clustering far from the turbine blades that is represented by the total number of elements. Three far region refinements have been considered with a total of 556850, 701600, and 943750 elements. For all the tested meshes, a fine wall-normal mesh resolution is maintained with a maximum dimensionless wall distance, y^+ of 2.5 and an average $y^+<1$. Although there are small differences in the prediction of the peak torque coefficient, as shown in Table 1, the baseline mesh with 701600 elements is considered to be sufficient for the analysis of the turbine performance with a reasonable computational cost.

Table 1 Mesh attributes and time step size sensitivity, including their effects on the cycle-averaged torque coefficient $\overline{C_T}$ and the peak torque coefficent $\widehat{C_T}$ for a single blade at the fifth cycle.

No.	Name	Features	No. of time steps per cycles [time step/cycle]	No. of nodes around the aerofoil	Total number of elements	$\overline{C_T}$	$\widehat{C_T}$
1			360			0.108	0.383
2	Mesh A1	Baseline mesh	540	1260	701600	0.108	0.383
3			1080			0.108	0.384
4	Mesh A2	Coarse chordwise	540	630	449600	0.109	0.383
5	Mesh A3	Fine chordwise		2520	1205600	0.107	0.382
6	Mesh A4	Fine far region mesh		1260	943750	0.108	0.383
7	Mesh A5	Coarse far region mesh		1260	556850	0.108	0.382

3.1.4 Model validation

Figure 12 shows a comparison between the current CFD prediction and both of the experimental and CFD data obtained by Li et al. [42] and this includes the torque coefficient distribution over one cycle from 0° to 360° of azimuthal angle. The experimental data are based on the integration of the pressure distribution obtained by the multiport pressure scanner fixed at the midsection of the blade. The comparison in Figure 12 shows that the proposed CFD model underpredicts the torque coefficient in the period between 0° and 60° of azimuthal angle, while it encounters an overprediction over the rest of the cycle. The main reason for the discrepancy between the experimental data and the current 2D CFD results is the exclusion of the 3D effects which include the effect of supporting struts and blade tip losses. In general, the 2D results over predict the power coefficient in contrast to the experimental data and the computationally expensive 3D CFD [49]. It may be noticed that the overprediction is much higher in the downstream part of the cycle, from 180° to 360° of azimuthal angle where the blade passes through the complex flow in the wake region. The azimuthal location of the CFD and experimental peak values are shifted by 5°, while the CFD data has a 15% higher peak. The comparisons with the set of CFD results from the literature [42] clarifies that the current 2D CFD results are reasonably accurate, especially in the downstream part of the cycle where complex flow structure exists. For more details, the predicted pressure

coefficient distributions around the blade at three azimuthal locations, namely 0°, 120°and 240°, are compared against the experimental data as shown in Figure 13 (a), (b), and (c). These comparisons show good agreement along the blade chord length, except near the leading edge where the solver overpredicts the negative pressure at the suction peak. These over predictions of the suction peak have many reasons, including the exclusion of the 3D effect and the assumption of a fully turbulent flow where could be a laminar zone near suction peak location [50]. These over predictions are reported for a range of computational methods including CFD [50]–[52]. Taking into account the complex and time-dependent aerodynamic characteristics of the flow around the VAWT, the proposed CFD model is considered suitable for the analysis of VAWTs.

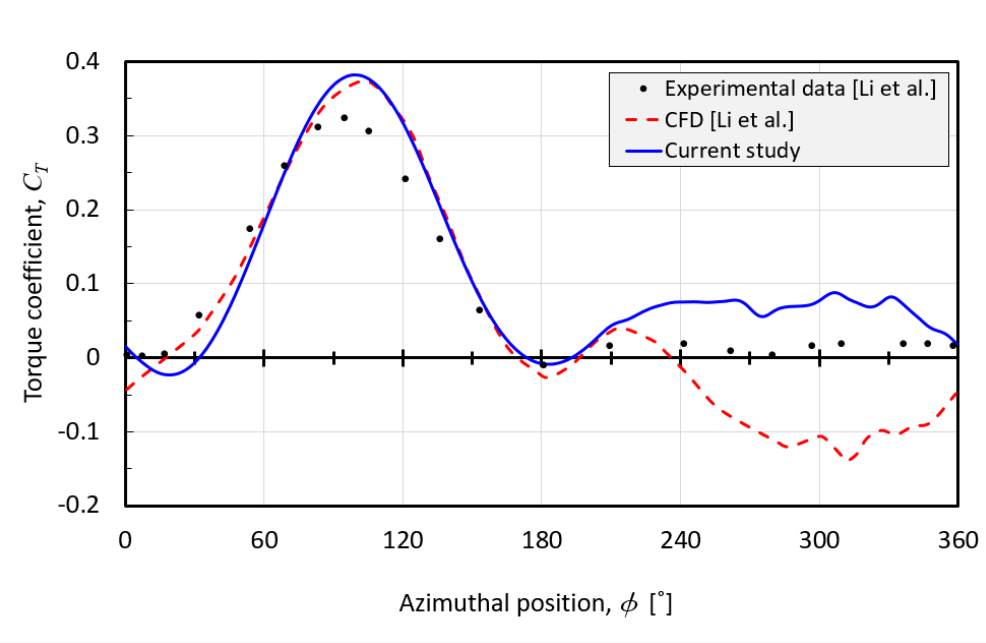

Figure 12 A comparison between the experimental and the numerical data for the single blade torque coefficient over a complete cycle.

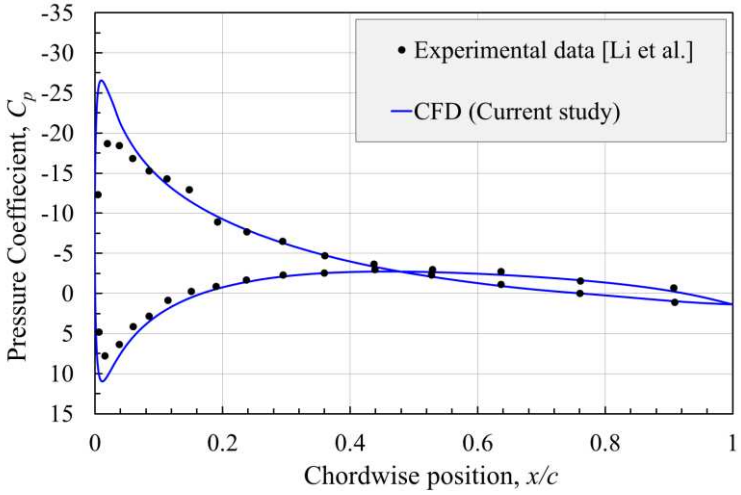

(a) θ=0˚

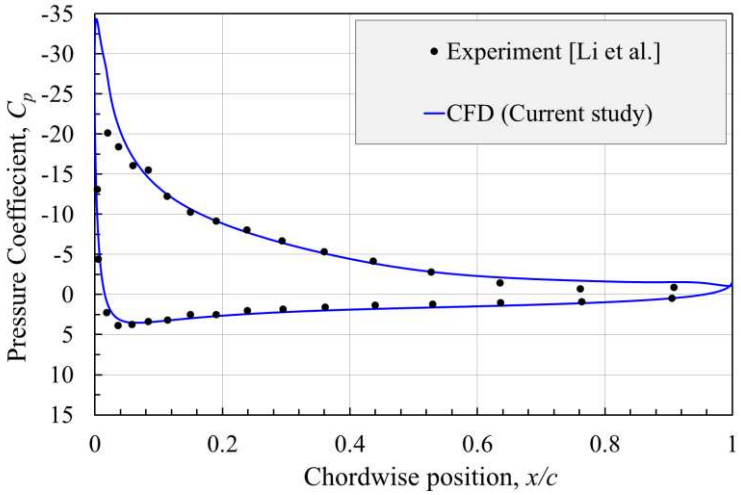

(b) θ=120˚

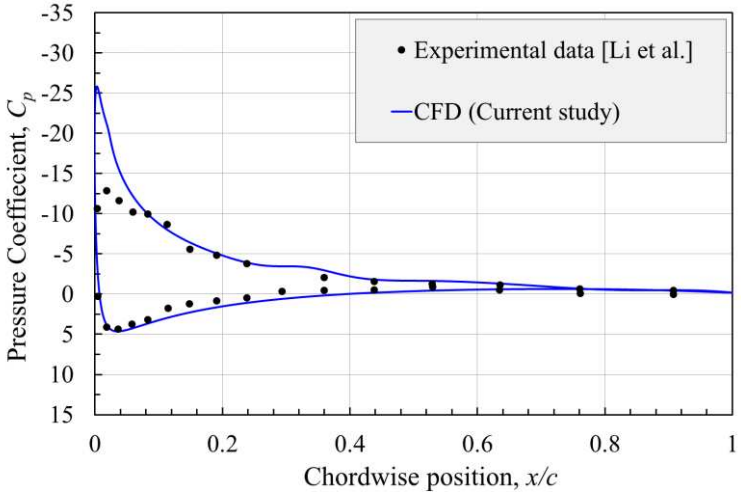

(c) θ=240˚

Figure 13 A comparison between the experimental and the numerical data of the pressure coefficient around the blade at azimuthal angles (a) 0°, (b) 120°, and (c) 240°.

3.2 Estimation of the AOA for a VAWT Blade

The simple analytical analysis of the AOA, α, is based on the assumption that the magnitude and direction of the approaching wind velocity, V, are constants and equal to that of the undisturbed flow velocity, V_∞. Figure 14 (a) illustrates the theoretical velocity triangle at the blade mount point for a zero fixed pitch turbine in an arbitrary azimuthal position, ϕ, and the blade rigid body velocity is represented by TSR* V_∞. Therefore, the local incident relative velocity, V_r, and the AOA, are simply defined as follows:

$$V_r = V\sqrt{sin^2\,\phi + (TSR + cos\,\phi)^2} \quad (1)$$

$$\alpha = tan^{-1}\frac{sin\,\phi}{TSR + cos\,\phi} \quad (2)$$

This calculation of the AOA is referred to as the theoretical AOA. However, in the real flow conditions, there are several phenomena that result in some distortion in both the magnitude and direction of the approaching wind velocity vector. These include the streamtube expansion, the flow deceleration in front of the turbine, and the blades wake interactions. A more realistic relative velocity triangle could be obtained by considering the variation of the magnitude and direction of the approaching wind velocity as shown in Figure 14 (b). A simple aerodynamic analysis could not achieve an accurate prediction of the AOA and the relative velocity magnitude. However, detailed CFD data could provide a good estimation of these quantities that could facilitate a better understanding of the turbine performance.

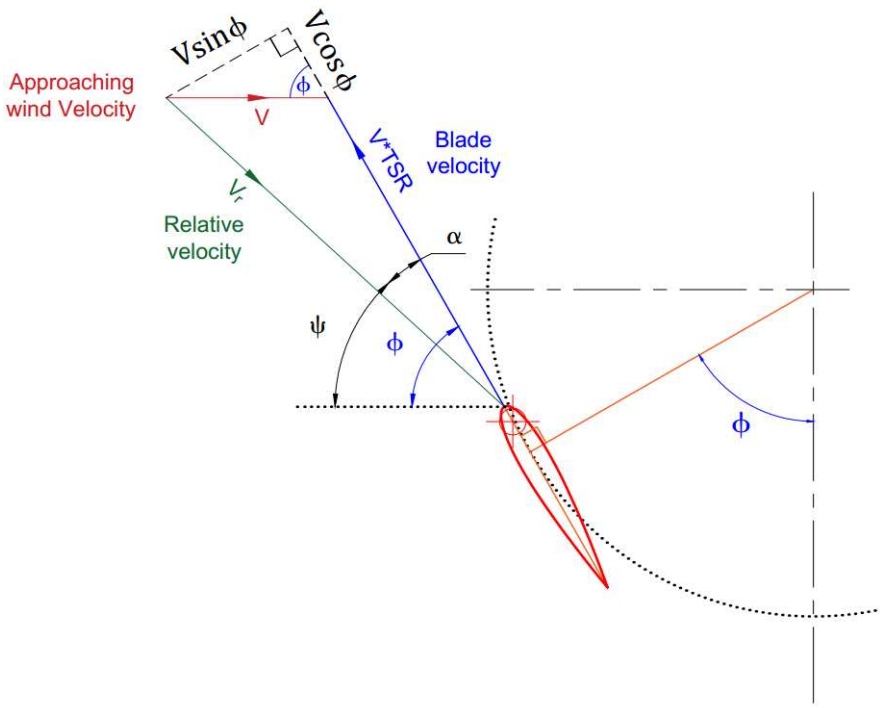

(a)

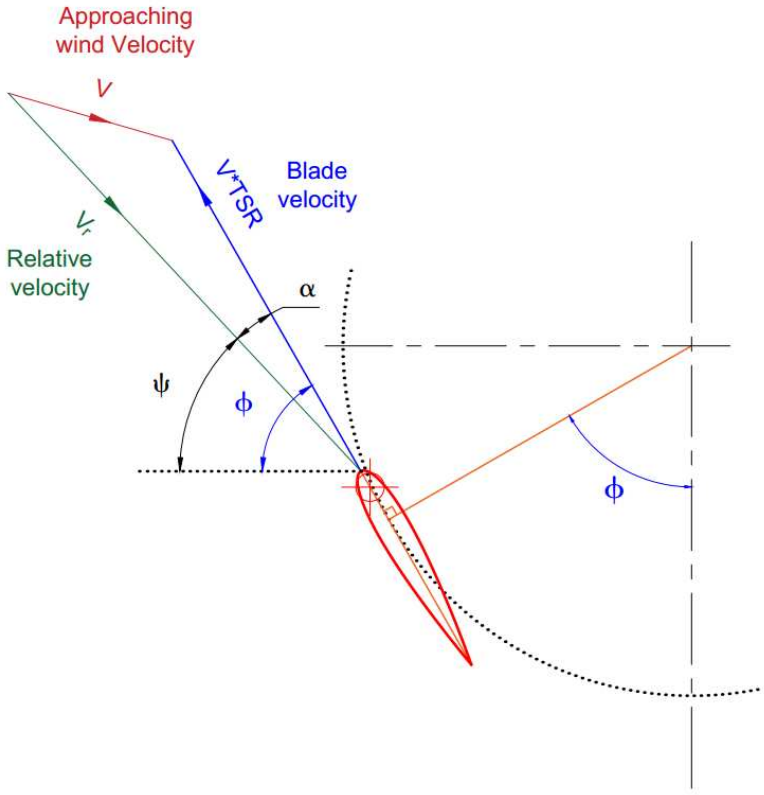

(b)

Figure 14 (a) A theoretical velocity triangle and (b) a realistic velocity triangle at an arbitrary azimuthal position. The angle of the approaching wind velocity in the realistic velocity triangle is arbitrarily chosen for illustration.

For the VAWT simulations, an interpreted UDF is hooked to the solver for the estimation of the AOA and the relative velocity magnitude. Firstly, the absolute velocity component is calculated at the suggested reference-points while the rigid body velocity of the blade is calculated at the blade mount point. Then, the AOA and the relative velocity magnitude are calculated and averaged between the pair of reference-points. Figure 15 shows a comparison between the theoretical AOA obtained using equation (2) and the estimated AOA based on the proposed method, over one cycle, for both zero fixed pitch (ZFP) and 6° fixed pitch (6° FP) configurations operating under the same condition as the validated test case. It is clear that the differences between the theoretical AOA and the estimated AOA are relatively smaller in the upstream part of the cycle, i.e. from 0° to 180° of azimuthal angle, and these differences are expected to be due to the streamtube expansion phenomenon. However, the differences in the downstream part of the cycle are dramatically higher due to the complexity of the turbine wake.

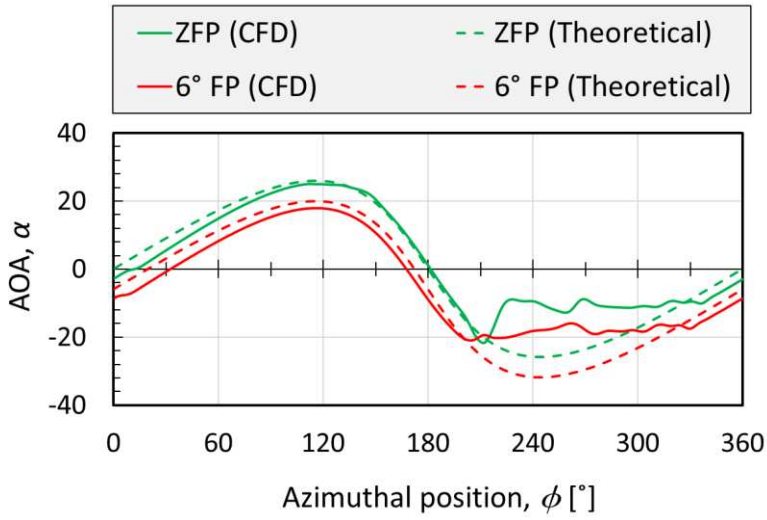

Figure 15 A comparison between the theoretical AOA and the estimated AOA based on the CFD data using the pair of reference-points for both of ZFP and 6°FP.

4 APPLICATION TO VARIABLE AND FIXED PITCH CONFIGURATIONS

The proposed AOA estimation method is used to evaluate the lift and drag coefficients for two test cases, namely the zero fixed pitch configuration and the sinusoidal variable pitch configuration. For simplicity, and from this point onward, zero fixed pitch and sinusoidal variable pitch will be referred to as ZFP and sinusoidal-VP, respectively. These pitch-configurations are simulated under the same geometrical and dynamical specifications as the validated test case in Section 3.1.4. The magnitude of the sinusoidal-VP is 11.9° and it is selected to equate to the difference between the maximum theoretical AOA of a ZFP turbine at a TSR of 2.29 and the favourable AOA of NACA0015 aerofoil that is assumed to be 14°. Five key characteristics have been considered and these include the instantaneous power coefficient, the AOA, the relative velocity magnitude, lift coefficient, and drag coefficient. Figure 16 illustrates the variations of these characteristics over a complete cycle, from 0° to 360° of azimuthal angle, for both of the ZFP and sinusoidal-VP configurations. The quantities plotted with the dashed lines and marked as theoretical are based on equations (1) and (2) and these are only plotted in the subfigures 16 (b) and (c). The VAWT under consideration has a two-bladed design but only one blade is considered for the analysis of the instantaneous power coefficient. The single-blade instantaneous power coefficient represents the generated power from a certain blade regardless of any other turbine component and hence could give more information on the performance of the blade in contrast with the instantaneous power coefficient of the whole turbine. The variation of the single-blade power coefficient for both of the ZFP and sinusoidal-VP are shown in Figure 16 (a). It is clear that the single-blade power coefficient of the sinusoidal-VP configuration is significantly higher in the period between 90° and 180°. However, the ZFP configuration has a higher single-blade power in the downstream part of the cycle, i.e. between 180° and 360°. The cycle-averaged single blade power coefficient is found to be 0.151 and 0.182 for

the ZFP and sinusoidal-VP, respectively. Hence, the sinusoidal-VP is able to improve the overall performance of the turbine by about 20% compared with the ZFP configuration under the current setup.

Figure 16 (b) shows the variation of both of the theoretical AOA and the estimated AOA based on the CFD data for both the ZFP and sinusoidal-VP. It may be noted that the implementation of the sinusoidal-VP significantly reduces the AOA so that it is almost within the favourable range in the upstream part of the cycle between 0° and 180°. However, the sinusoidal-VP results in a considerably lower AOA in the downstream part of the cycle. The theoretical relative velocity magnitude and its estimated values based on CFD data are compared in Figure 16 (c) for both of the ZFP and sinusoidal-VP. While the differences between the theoretical and the CFD based values are minimal in the upstream part of the cycle, there are considerable differences in the downstream part due to the distortion of the flow in the wake region. The subfigures Figure 16 (d) and (f) show the variation of the lift and drag coefficients, respectively, for both the ZFP and sinusoidal-VP. Due to the aerodynamic characteristics of the VAWT, both the favourable AOA and lift coefficient are negative in the downstream part of the cycle. In addition, the aerodynamic definition of the drag forces illustrates that it is always positive. Therefore, any negative value in the estimated drag coefficient is considered as an error. The reason for these negative values is that any slight miscalculation of the AOA may result in adding a fraction of the relatively higher negative lift component into the drag coefficient. Considering the variations of the lift and drag coefficients along with the AOA, it is clear that the ZFP blade encounters a severe stall condition between 90° and 140° and this is characterized by a high AOA followed by a sudden reduction in the lift and drag coefficients. Although the ZFP blade has a higher lift coefficient in the period between 90 and 140°, its power coefficient is dramatically lower. The reason is that the large drag forces in this period act to significantly reduce the tangential force and hence reduce both the driving torque and the power

coefficient. On the other hand, the sinusoidal-VP blade operates at a favourable AOA and produces a lower lift coefficient while maintaining a significantly lower drag coefficient and this is in contrast with that of the ZFP blade in the upstream part of the cycle. This enables the sinusoidal-VP blade to achieve a better power coefficient distribution over the upstream part of the cycle. However, in the downstream part of the cycle, the ZFP blade obtains a higher lift coefficient with a negligible drag due to its better AOA potential. These favourable lift and drag coefficients illustrate how the ZFP configuration obtains a higher power coefficient over the downstream part of the cycle.

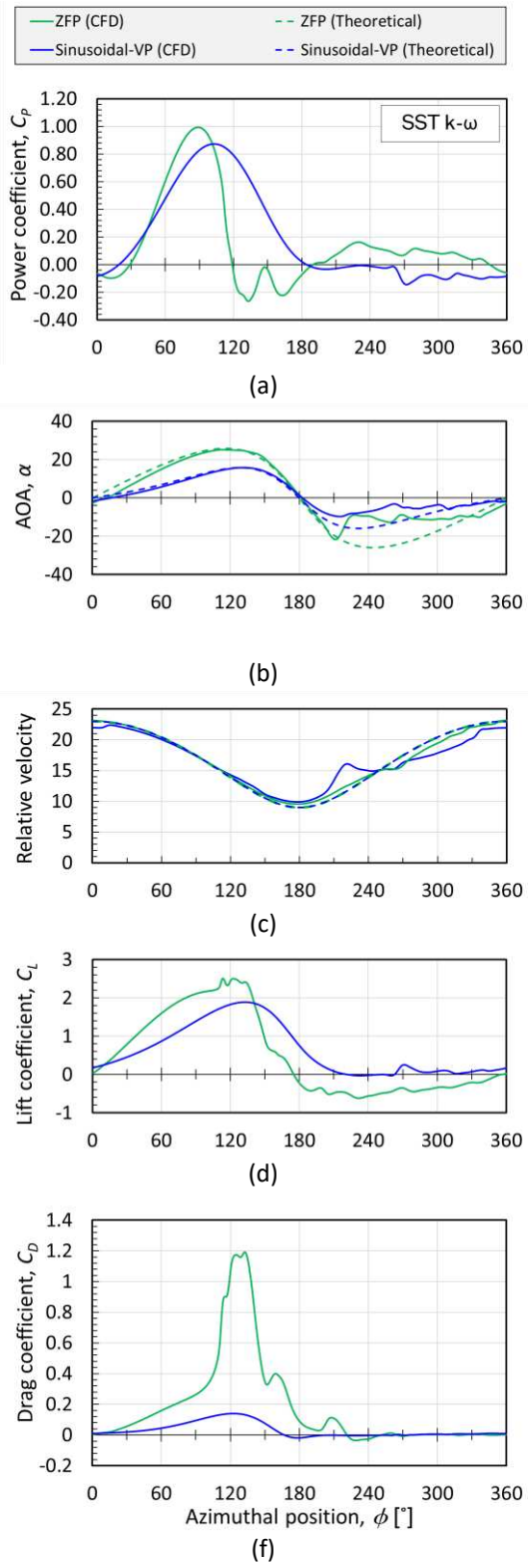

Figure 16 A comparison between the ZFP and sinusoidal-VP VAWTs according to (a) the instantaneous power coefficient, (b) AOA, (c) relative velocity magnitude, (d) lift coefficient, and (f) drag coefficient (the horizontal axis of all the subfigures represents the azimuthal position).

5 CONCLUSIONS

The distribution of the AOA over the entire cycle has significant effects on the overall power coefficient of the VAWT and this makes the proper estimation of the AOA essential. Due to the very complex flow across the VAWT, several ways of selecting the reference-points for the estimation of the AOA have been investigated and it is found that using the flow data from the two reference points at the locations 0.5 aerofoil chord length upstream and 1 chord away from each side of the aerofoil can give most accurate estimation across a range of operating conditions. The new method could be used to calculate and store the AOA data during the CFD simulations without the need for extensive post-processing. In comparison with existing method in the literate, the proposed method can reduces the RMSE by as much as an average of 33.8% for the three tested flow velocities relent to small wind turbine conditions. Based on the proposed AOA estimation method, the performance of a fixed pitch and the sinusoidal variable pitch VAWT configurations have been analysed and it illustrated how the sinusoidal variable pitch configuration could enhance the overall performance of the turbine by maintaining more favourable AOAs to maximise the lift and reduce the drag generation. The method could be used for efficient turbine aerodynamic analysis and optimisation of VAWT.

ACKNOWLEDGEMENT

Mohamed M. Elsakka would like to express his gratitude to the Egyptian Cultural Affairs and Missions Sector along with Port Said University for their financial support.

6 REFERENCES

[1] M. R. Islam, S. Mekhilef, and R. Saidur, "Progress and recent trends of wind energy technology," *Renewable and Sustainable Energy Reviews*, vol. 21, pp. 456–468, May 2013.

[2] D. Marten, A. Bianchini, G. Pechlivanoglou, F. Balduzzi, C. N. Nayeri, G. Ferrara, C. O. Paschereit, and L. Ferrari, "Effects of Airfoil's Polar Data in the Stall Region on the Estimation of Darrieus Wind Turbine Performance," *Journal of Engineering for Gas Turbines and Power*, vol. 139, no. 2, pp. 1–9, Sep. 2016.

[3] W. Tjiu, T. Marnoto, S. Mat, M. H. Ruslan, and K. Sopian, "Darrieus vertical axis wind turbine for power generation II: Challenges in HAWT and the opportunity of multi-megawatt Darrieus VAWT development," *Renewable Energy*, vol. 75, pp. 560–571, Mar. 2015.

[4] S. Bhuyan and A. Biswas, "Investigations on self-starting and performance characteristics of simple H and hybrid H-Savonius vertical axis wind rotors," *Energy Conversion and Management*, vol. 87, pp. 859–867, Nov. 2014.

[5] S. Bhattacharjee and S. Acharya, "Performative analysis of an eccentric solar–wind combined system for steady power yield," *Energy Conversion and Management*, vol. 108, pp. 219–232, Jan. 2016.

[6] M. Ghasemian, Z. N. Ashrafi, and A. Sedaghat, "A review on computational fluid dynamic simulation techniques for Darrieus vertical axis wind turbines," *Energy Conversion and Management*, vol. 149, pp. 87–100, Oct. 2017.

[7] J. M. Edwards, L. A. Danao, and R. J. Howell, "Novel Experimental Power Curve Determination and Computational Methods for the Performance Analysis of Vertical Axis Wind Turbines," *Journal of Solar Energy Engineering*, vol. 134, pp. 1–11, 2012.

[8] M. Somoano and F. J. Huera-Huarte, "The dead band in the performance of cross-flow turbines: Effects of Reynolds number and blade pitch," *Energy Conversion and Management*, vol. 172, pp. 277–284, Sep. 2018.

[9] P. Jain and A. Abhishek, "Performance prediction and fundamental understanding of small scale vertical axis wind turbine with variable amplitude blade pitching," *Renewable Energy*, vol. 97, pp. 97–

113, Nov. 2016.

[10] T. Kiwata, T. Kita, T. Yamada, S. Takata, N. Komatsu, and S. Kimura, “Performance of vertical axis wind turbine with variable-pitch straight blades by a linkage mechanism,” *Transactions of the Japan Society of Mechanical Engineers Series B*, vol. 74, no. 748, pp. 2543–2551, 2010.

[11] C. Xisto, J. Páscoa, and M. Trancossi, “Numerical analysis of design parameters with strong influence on the aerodynamic efficiency of a small-scale self-pitch VAWT,” in *Volume 1: Advances in Aerospace Technology*, 2015, pp. 1–11.

[12] T. Yamada, T. Kiwata, T. Kita, M. Hirai, N. Komatsu, and T. Kono, “Overspeed control of a variable-pitch vertical-axis wind turbine by means of tail vanes,” *Journal of Environment and Engineering*, vol. 7, no. 1, pp. 39–52, 2012.

[13] D. W. Erickson, J. J. Wallace, and J. Peraire, “Performance characterization of cyclic blade pitch variation on a vertical axis wind turbine,” in *49th AIAA Aerospace Sciences Meeting*, 2011, pp. 1–23.

[14] L. Liu, C. Liu, and X. Zheng, “Modeling, simulation, hardware implementation of a novel variable pitch control for H-type vertical axis wind turbine,” *Journal of Electrical Engineering*, vol. 66, no. 5, pp. 264–269, Jan. 2015.

[15] I. Paraschivoiu, O. Trifu, and F. Saeed, “H-Darrieus wind turbine with blade pitch control,” *International Journal of Rotating Machinery*, vol. 2009, pp. 1–7, 2009.

[16] B. Shahizare, N. Nik-Ghazali, W. T. Chong, S. Tabatabaeikia, N. Izadyar, and A. Esmaeilzadeh, “Novel investigation of the different omni-direction-guide-vane angles effects on the urban vertical axis wind turbine output power via three-dimensional numerical simulation,” *Energy Conversion and Management*, vol. 117, pp. 206–217, 2016.

[17] R. Gosselin, G. Dumas, and M. Boudreau, “Parametric study of H-Darrieus vertical-axis turbines using CFD simulations,” *Journal of Renewable and Sustainable Energy*, vol. 8, no. 5, pp. 1–22, Sep. 2016.

[18] Z. Wang and M. Zhuang, “Leading-edge serrations for performance improvement on a vertical-axis wind turbine at low tip-speed-ratios,” *Applied Energy*, vol. 208, pp. 1184–1197, Dec. 2017.

[19] H. Lei, D. Zhou, Y. Bao, Y. Li, and Z. Han, “Three-dimensional Improved Delayed Detached Eddy

Simulation of a two-bladed vertical axis wind turbine," *Energy Conversion and Management*, vol. 133, pp. 235–248, Feb. 2017.

[20] Z. Wang, Y. Wang, and M. Zhuang, "Improvement of the aerodynamic performance of vertical axis wind turbines with leading-edge serrations and helical blades using CFD and Taguchi method," *Energy Conversion and Management*, vol. 177, pp. 107–121, Dec. 2018.

[21] A. Rezaeiha, H. Montazeri, and B. Blocken, "Towards accurate CFD simulations of vertical axis wind turbines at different tip speed ratios and solidities: Guidelines for azimuthal increment, domain size and convergence," *Energy Conversion and Management*, vol. 156, pp. 301–316, Jan. 2018.

[22] S. Ali, S. M. Lee, and C. M. Jang, "Effects of instantaneous tangential velocity on the aerodynamic performance of an H-Darrieus wind turbine," *Energy Conversion and Management*, vol. 171, pp. 1322–1338, Sep. 2018.

[23] A. Bianchini, G. Ferrara, and L. Ferrari, "Design guidelines for H-Darrieus wind turbines: Optimization of the annual energy yield," *Energy Conversion and Management*, vol. 89, pp. 690–707, Jan. 2015.

[24] C. E. Soraghan, W. E. Leithead, H. Yue, and J. Feuchtwang, "Double multiple streamtube model for variable pitch vertical axis wind turbines," in *43rd AIAA Fluid Dynamics Conference and Exhibit*, 2013, pp. 1–12.

[25] F. Kanyako and I. Janajreh, "Vertical axis wind turbine performance prediction, high and low fidelity analysis," in *The 2014 IAJC-ISAM International Conference*, 2014, pp. 1–14.

[26] N. C. K. Pawsey, "Development and evaluation of passive variable-pitch vertical axis wind turbines," PhD dissertation, The University of New South Wales, 2002.

[27] L. B. Wang, L. Zhang, and N. D. Zeng, "A potential flow 2-D vortex panel model: Applications to vertical axis straight blade tidal turbine," *Energy Conversion and Management*, vol. 48, no. 2, pp. 454–461, Feb. 2007.

[28] A. Bianchini, F. Balduzzi, P. Bachant, G. Ferrara, and L. Ferrari, "Effectiveness of two-dimensional CFD simulations for Darrieus VAWTs: a combined numerical and experimental assessment," *Energy Conversion and Management*, vol. 136, pp. 318–328, Mar. 2017.

[29] R. Shrivastava, “Efficiency improvement of a straight-bladed vertical axis wind turbine,” *People’s Journal of Science & Technology*, vol. 2, no. 1, pp. 16–19, 2012.

[30] R. Firdaus, T. Kiwata, T. Kono, and K. Nagao, “Numerical and experimental studies of a small vertical-axis wind turbine with variable-pitch straight blades,” *Journal of Fluid Science and Technology*, vol. 10, no. 1, pp. 1–15, 2015.

[31] Z. Q. Yao and C. L. Yang, “Numerical simulation of unsteady flow for variable-pitch vertical axis wind turbine,” *Applied Mechanics and Materials*, vol. 291–294, pp. 490–495, 2013.

[32] M. Elkhoury, T. Kiwata, and E. Aoun, “Experimental and numerical investigation of a three-dimensional vertical-axis wind turbine with variable-pitch,” *Journal of Wind Engineering and Industrial Aerodynamics*, vol. 139, pp. 111–123, 2015.

[33] Z. Wu, Y. Cao, S. Nie, and Y. Yang, “Effects of rain on vertical axis wind turbine performance,” *Journal of Wind Engineering and Industrial Aerodynamics*, vol. 170, pp. 128–140, Nov. 2017.

[34] C. Li, S. Zhu, Y. Xu, and Y. Xiao, “2.5D large eddy simulation of vertical axis wind turbine in consideration of high angle of attack flow,” *Renewable Energy*, vol. 51, pp. 317–330, Mar. 2013.

[35] M. F. Ismail and K. Vijayaraghavan, “The effects of aerofoil profile modification on a vertical axis wind turbine performance,” *Energy*, vol. 80, pp. 20–31, Feb. 2015.

[36] M. S. Campobasso, J. Drofelnik, and F. Gigante, “Comparative assessment of the harmonic balance Navier–Stokes technology for horizontal and vertical axis wind turbine aerodynamics,” *Computers & Fluids*, vol. 136, pp. 354–370, Sep. 2016.

[37] S. Wang, D. B. Ingham, L. Ma, M. Pourkashanian, and Z. Tao, “Numerical investigations on dynamic stall of low Reynolds number flow around oscillating airfoils,” *Computers & Fluids*, vol. 39, no. 9, pp. 1529–1541, Oct. 2010.

[38] P. Kozak, “Blade pitch optimization methods for vertical-axis wind turbines,” Illinois Institute of Technology, 2016.

[39] A. Bianchini, F. Balduzzi, G. Ferrara, and L. Ferrari, “Virtual incidence effect on rotating airfoils in Darrieus wind turbines,” *Energy Conversion and Management*, vol. 111, pp. 329–338, Mar. 2016.

[40] H. Youngren and M. Drela, “Xfoil subsonic airfoil development system.” Open source software available at http://web. mit. edu/drela/Public/web/xfoil, 2005.

[41] J. Morgado, R. Vizinho, M. A. R. Silvestre, and J. C. Páscoa, “XFOIL vs CFD performance predictions for high lift low Reynolds number airfoils,” *Aerospace Science and Technology*, vol. 52, pp. 207–214, May 2016.

[42] Q. Li, T. Maeda, Y. Kamada, J. Murata, T. Kawabata, K. Shimizu, T. Ogasawara, A. Nakai, and T. Kasuya, “Wind tunnel and numerical study of a straight-bladed vertical axis wind turbine in three-dimensional analysis (Part I: For predicting aerodynamic loads and performance),” *Energy*, vol. 106, pp. 443–452, 2016.

[43] L. Battisti, L. Zanne, S. Dell’Anna, V. Dossena, G. Persico, and B. Paradiso, “Aerodynamic measurements on a vertical axis wind turbine in a large scale wind tunnel,” *Journal of Energy Resources Technology*, vol. 133, no. 3, pp. 1–9, 2011.

[44] Q. Li, T. Maeda, Y. Kamada, J. Murata, K. Shimizu, T. Ogasawara, A. Nakai, and T. Kasuya, “Effect of solidity on aerodynamic forces around straight-bladed vertical axis wind turbine by wind tunnel experiments (depending on number of blades),” *Renewable Energy*, vol. 96, pp. 928–939, 2016.

[45] B. Paillard, J.-A. Astolfi, and F. Hauville, “CFD simulation and experimental validation of a vertical axis turbine: toward variable pitch cross-flow marine turbine for maximizing hydropower extraction—the SHIVA project,” in *Volume 5: Ocean Space Utilization; Ocean Renewable Energy*, 2011, pp. 619–627.

[46] D. W. Wekesa, C. Wang, Y. Wei, and L. A. M. Danao, “Influence of operating conditions on unsteady wind performance of vertical axis wind turbines operating within a fluctuating free-stream: A numerical study,” *Journal of Wind Engineering and Industrial Aerodynamics*, vol. 135, pp. 76–89, 2014.

[47] ANSYS Inc., “ANSYS FLUENT User’s Guide,” Canonsburg, 2013.

[48] M. Yi, Q. Jianjun, and L. Yan, “Airfoil design for vertical axis wind turbine operating at variable tip speed ratios,” *The Open Mechanical Engineering Journal*, vol. 9, pp. 1007–1016, 2015.

[49] B. Hand and A. Cashman, “Aerodynamic modeling methods for a large-scale vertical axis wind turbine: A comparative study,” *Renewable Energy*, vol. 129, pp. 12–31, Dec. 2018.

[50] C. P. van Dam, D. D. Chao, and D. E. Berg, “CFD analysis of rotating two-bladed flatback wind turbine rotor.,” Apr. 2008.

[51] B. Nelson and J.-S. Kouh, “The numerical analysis of wind turbine airfoils at high angles of attack,” *International Journal of Energy and Environmental Engineering*, vol. 7, no. 1, pp. 1–12, Mar. 2016.

[52] D. Baldacchino, M. Manolesos, C. Ferreira, Á. González Salcedo, M. Aparicio, T. Chaviaropoulos, K. Diakakis, L. Florentie, N. R. García, G. Papadakis, N. N. Sørensen, N. Timmer, N. Troldborg, S. Voutsinas, and A. van Zuijlen, “Experimental benchmark and code validation for airfoils equipped with passive vortex generators,” *Journal of Physics: Conference Series*, vol. 753, no. 2, Sep. 2016.